Research Paper

Microstructural Aspects in the Diffusion Bonding of Zr702 to A516 Steel with Ni/Mo/Ti Multi-Interlayer

Ali Pourjafar[1], Seyed Reza Alavi Zaree[2*], Reza Dehmolaei[3], Khalil Ranjbar[4], Mohammadreza Tavakoli Shoushtari[5]

1. PhD candidate, Department of Materials Science & Engineering, Faculty of Engineering, Shahid Chamran University of Ahvaz, Ahvaz, Iran.

2. Associate Professor, Department of Materials Science & Engineering, Faculty of Engineering, Shahid Chamran University of Ahvaz, Ahvaz, Iran.

3. Associate Professor, Department of Materials Science & Engineering, Faculty of Engineering, Shahid Chamran University of Ahvaz, Ahvaz, Iran.

4. Professor, Department of Materials Science & Engineering, Faculty of Engineering, Shahid Chamran University of Ahvaz, Ahvaz, Iran.

5. Assistant Professor, Department of Materials Science & Engineering, Faculty of Engineering, Shahid Chamran University of Ahvaz, Ahvaz, Iran.

ARTICLE INFO

ABSTRACT

The bonding of zirconium to various grades of steel has found increasing applications in different industries. Due to their fusion welding problems, the solid state bonded joints of these alloys have received more attention from researchers. In this study, diffusion bonding between zirconium alloy Zr702 and low-alloy steel A516 was performed using a multi-layer interlayer consisting of titanium, molybdenum, and nickel. The bonding process was carried out at a temperature range of 900-1050℃ for 30 minutes using the spark plasma diffusion bonding method. The microstructure and interdiffusion of elements at different interfaces were examined using a field emission scanning electron microscope (FESEM) equipped with EDS analysis. The results showed that a suitable bonded joint was successfully established with the interlayers arranged as Zr702/Ti/Mo/Ni/Steel. At the interface of the interlayers with the base metals, no harmful phases, cracks, or discontinuities were observed. In the Zr/Ti joint interface, diffusion zones were identified as $(\alpha+\beta)$ (Zr,Ti), β(Ti,Zr), and α(Ti,Zr). In the Ti/Mo interface, two solid solution diffusion zones were present, while the Mo/Ni interface showed two areas that included solid solutions and intermetallic phases. In the Ni/A516 joint interface, a solid solution combination and an intermetallic composition were identified. EDS Linear analysis results indicated that the maximum diffusion occurred in the Zr/Ti layer, while the lowest diffusion was observed in the Ti/Mo layer.

* **Corresponding Author:**
E-Mail: sr.alavizaree@scu.ac.ir

Introduction

Zirconium 702, known as commercial pure zirconium, is one of the most popular structural materials due to its excellent mechanical properties, outstanding corrosion resistance, and good machinability. It is used in various industries, including nuclear energy production, petrochemicals, medical applications, and in structures exposed to severely corrosive environments, such as towers, reactors, heat exchangers, steam generators, pumps, piping systems, valves, and agitators [1-2]. Due to the diverse application of Zr in different industries, dissimilar welding of this material to other alloys is a matter of concern. The bonding of zirconium alloys and steels, especially stainless steels, is widely used in various industries [3-5].

Despite the good weldability of zirconium alloys, fusion welding of these alloys with steels showed problems such as segregation, formation of undesired phases and brittle intermetallic compounds (Zr-Cr, Zr-Fe, Zr-Ni), grain growth in the fusion zone and heat-affected zone (HAZ), and the possibility of non-uniform twisting and distortion [6]. These problems can cause a severe reduction in the properties of plasticity and strength of the joints and damage the performance of the bonded joints [7]. Solid-state welding methods, such as diffusion bonding, are a good alternative to fusion welding of zirconium alloys, especially in dissimilar states with other alloys, such as steels, to overcome some of the mentioned problems [8]. Due to the difference in physical and mechanical properties and chemical composition of metals and alloys, their diffusion bonding, especially in dissimilar states, faces important challenges. Some of these challenges (especially in dissimilar states) are: 1) forming brittle and undesirable intermetallic compounds at the interface of the bonding, 2) thermal residual stresses due to the difference in the thermal expansion coefficient of the base metals, 3) lack of formation of a suitable diffusion layer due to the difference in interdiffusion of atoms and the limitation of solid-state diffusion [9].

Meanwhile, the control of process parameters such as temperature, time, bonding pressure, and the use of a suitable interlayer play a key role in reducing defects [10-11]. Using a suitable interlayer can help to create a good bond by increasing the effective contact surface, reducing residual stresses, and preventing the formation of undesirable intermetallic compounds [12]. Diffusion bonding is highly dependent on temperature, and as temperature increases, the diffusion depth of atoms and the thickness of the reactive layer increase [13].

Insufficient bonding temperature can also cause insufficient diffusion and lack of proper reaction layer formation and decrease bonding properties [14]. Nevertheless, an excessive increase in diffusion bonding temperature can increase thermal residual stresses in the interface and encourage the formation of harmful intermetallic phases and compounds and, as a result, reduce the joint properties [15]. Therefore, the control and correct selection of the bonding temperature in diffusion bonding is of particular importance. The spark plasma diffusion bonding method (SPDB) can be used for solid-state welding. This method is based on the spark plasma sintering (SPS) technique, which increases the diffusion of atoms and improves the conditions of plastic deformation at the interface of base metals and interlayers. The main advantage of SPDB is the high heating rate in the joint interface, which makes it more significant than previous methods [16]. Reducing the bonding time compared to other methods, higher heating rate, ease of use, high local heating at the joint interface of the samples, and avoiding oxidation of the sample due to the use of protective atmospheres (neutral environment or vacuum) are benefits of the SPDB route [17]. In this research, the effect of bonding temperature and the use of multiple Ni/Mo/Ti interlayers on the microstructural aspects and interdiffusion of atoms of the Zr702 and A516 bonded joint with the (SPDB) technique have been studied and investigated, and the combination of multiple interlayers compatible with base metals and the best diffusion bonding temperature was introduced.

2. Experimental Procedure

Discs of Zr 702 and steel A516 with 23.5 mm in diameter and thicknesses of 2.8 and 3.1 mm, respectively, were used as base metals. Table 1 shows the chemical composition of the base metals used. Titanium, nickel, and molybdenum foils with high purity, a thickness of 100 μm, and the same diameter as the base material were used as interlayers. The base metals and the interlayers were sanded with SiC papers up to 5000 and polished using 0.05-micron alumina powder and diamond paste. Any contamination on the surfaces is removed using acetone. The bonding was done using the spark plasma diffusion bonding (SPDB) technique with a spark plasma sintering (SPS) device. For this purpose, the base metals and the interlayers, respectively, Zr702/Ti/Mo/Ni/A516, were carefully placed on top of each other and placed in the SPS machine (Figures 1-a and 1-b). The samples were heated in the SPS device at a rate of 20 °C/min until reaching the bonding temperature (Figure 1-c). The bonding of the joints was done at 1050, 1000, 950, and 900 °C for 30 minutes under a vacuum of 0.05 mbar. For microstructural studies, suitable samples of the manufactured joints were prepared using a wire

cutting machine. The cross section of the samples was sanded using 120 to 5000 grits, then polished using 0.05-micron alumina powder and etched with a 10HF-45HNO₃-10H₂O (mL) solution. The different interfaces of base metals and interlayers were studied and investigated using an SEM microscope. Further microstructural studies and phase analysis were done using a FESEM field emission electron microscope equipped with a MIRA3-TESCAN EDS analysis system. The diffusion depth of atoms and the thickness of reactive layers in different joints were measured by Digimizer scale measurement software.

Table 1. Chemical composition of base metals (wt %)

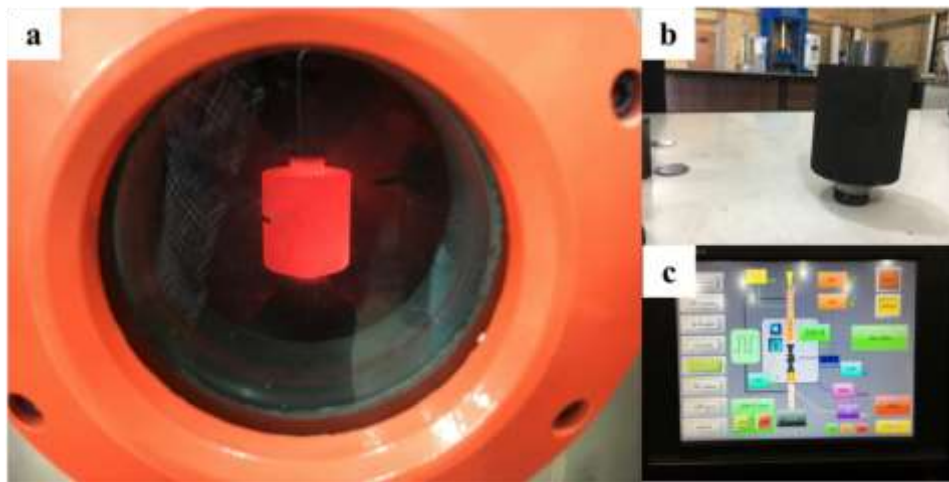| Alloy	Zr+Hf (Min)	Hf (Max)	C	Nb	Fe	Cr/Ni/Cu	Fe+Cr Max	Mn	O (Max)	Si	P/S/Ti
Zr702	99.2	4.5	-	-	-	-	0.2	-	0.16	-	-
A516	-	-	0.1~0.22	0.01	Base	0.3	-	1~1.7	-	0.6	0.03

Fig. 1. Used equipment: Placement of samples in the SPS device

3. Results and discussion

Figure 2 shows FESEM images and EDS linear analysis of Zr702/Ti joint interfaces at different temperatures. The figure clearly shows that at all temperatures the interdiffusion of titanium and zirconium atoms has been done well and the reaction layer has been formed. From Figure 2-A, two separate regions, I and II, can be identified in the reaction layer formed at 900 ℃. The thickness of the reactive layer is higher on the Ti side, which can be attributed to the higher rate of diffusion of titanium atoms compared to zirconium [18]. The results of linear EDS analysis in Figure 2-B show the proper interdiffusion of titanium and zirconium atoms. The trend of changing the chemical composition of the elements in this figure revealed that both regions I and II are solid solutions of Zr in Ti and Ti in Zr, and no intermetallic compounds have been formed. Considering the atomic radii difference of Zr and Ti (that is less than 15%), as well as the Zr-Ti phase equilibrium diagram, it is concluded that these two elements have good solubility at all temperatures, and while forming a predicted solid solution, no intermetallic compounds are formed in their interface [13,18]. The region I in the vicinity of Zr702 is defined as a two-phase region including $\alpha_{(Zr,Ti)}$ solid solution in the matrix of $\beta_{(Zr,Ti)}$ solid solution (needle-shaped phases in light gray field). As Hafnium is a $\beta_{(Zr,Ti)}$ phase stabilizer and presence of nearly 4.5% of Hf in the chemical composition of Zr702, it could play a decisive role in the stability of this phase [19]. Based on the results of EDS analysis and Ti-Zr phase diagram, region II (light gray areas and parallel or needle-shaped dendrites), could be identified as dendritic regions in the joint interface with the same solid solution composition of $\alpha_{(Ti,Zr)}$ and $\beta_{(Ti,Zr)}$ phases. The results of the EDS analysis show that the areas adjacent to the Zr50%-Ti50% composition are composed of $/\beta_{(Ti,Zr)}/\beta_{(Zr,Ti)}$ and in the vicinity of the titanium interlayer, the (α+β)(Ti, Zr) phase is formed in the form of layers, with a dark gray color and a lamellar structure rich in titanium. Figure 4-A also shows that with the increase of Ti diffusion, a higher density of dendrites can be seen in

this area. Similar results have been reported by other researchers [12,18].

It can be seen from Figures 4-C and 4-D that the reactive layer is well formed at the bonding temperature of 950 ℃. Similar to the temperature of 900 ℃, at this temperature, two regions, I and II, are visible in the reactive layer. Increasing the bonding temperature by 50 ℃ does not cause new compounds and phases to form at the Zr/Ti interface, and only the depth of interdiffusion of atoms (thickness of the reactive layer) has increased. This finding has been confirmed by the results of linear EDS analysis in Figure 4-D. Comparing the images of Figures 2-A and 2-C shows that as process temperature increased, the thickness of the plates (needle-shaped areas) increased and their density decreased. In fact, with the increase of the bonding temperature, the depth and diffusion rate of titanium atoms increase, and the concentration of titanium atoms decreases in these areas, and this causes a decrease in the needles density and an increase in their thickness near the zirconium base metal. Similar results have been reported by other researchers [18,20-21].
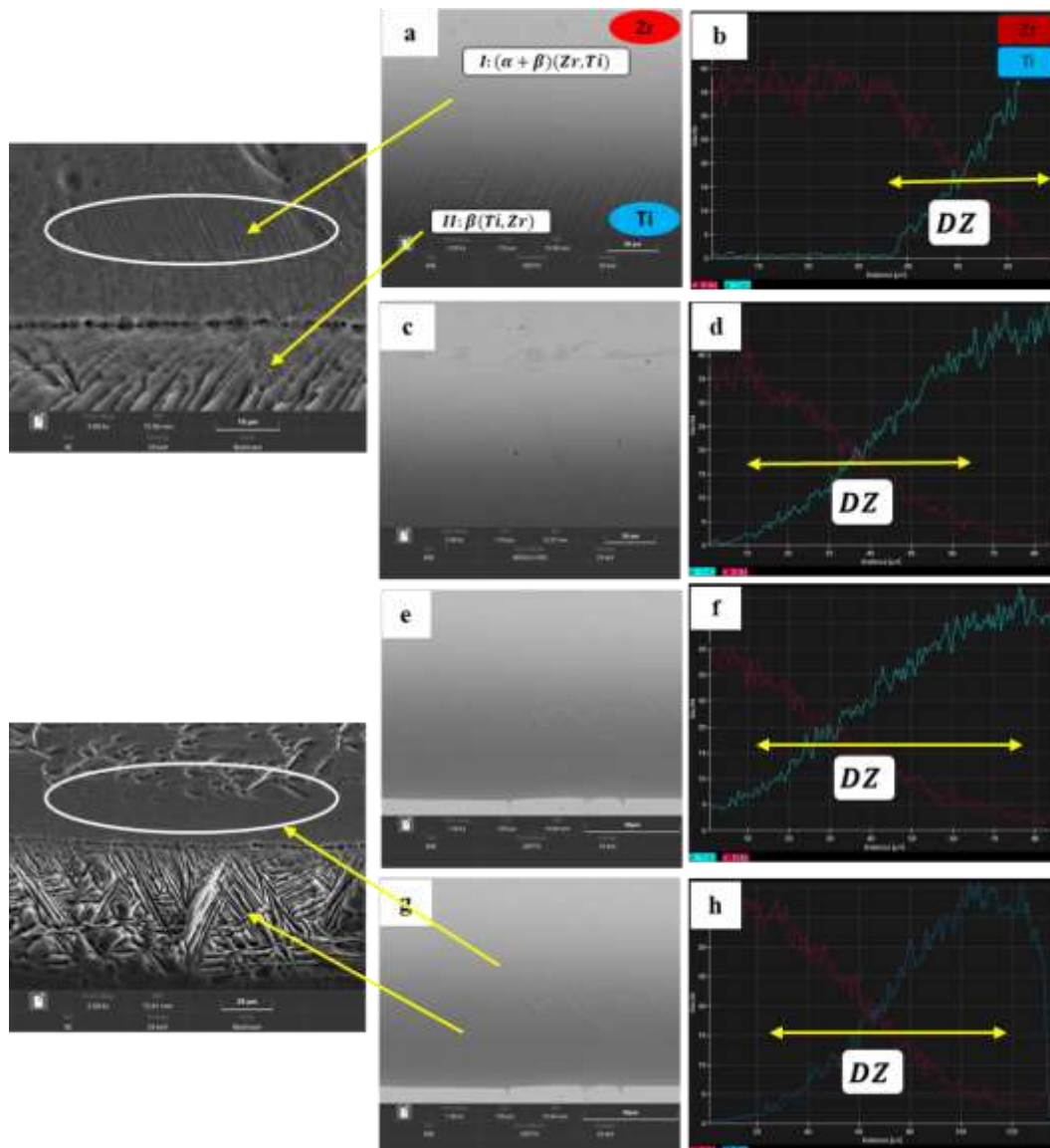

Fig. 2. FESEM images and EDS analysis of Zr702/Ti bonding interface at different temperatures A-B- 900 ℃ C-D- 950 ℃ E-F- 1000 ℃ G-H- 1050 ℃

At the interface of Zr702/Ti formed at bonding temperatures of 1000℃ and 1050℃ (Figures 2-E and 2-G) no defects are revealed, and the same as at lower temperatures, two distinct areas, II and I, could be clearly distinguished. The depth of interdiffusion of titanium and zirconium atoms (the thickness of the reactive layer) has increased at higher temperatures so that it is visible and verified by linear EDS analysis in Figure 2-F and Figure 2-H. At higher temperatures of bonding, the density of the needle-shaped areas (α(Zr,Ti) phase) near the Zr702 base metal has decreased and their thickness has increased. Based on

the fact that diffusion is a time- and temperature-dependent process (equations 1 and 2), the diffusion rate of atoms increases exponentially with temperature increase. Therefore, as the temperature increases, the thickness of the reactive layers also increases. The growth of the reactive layer can follow the parametric growth law according to equations 1 and 2 [22-23].

$$X^2 = Dt \tag{1}$$

$$D = D_0 \exp(-Q/RT) \tag{2}$$

In this equation, X is the thickness of the reactive layer (interdiffusion depth of atoms, meters), D is the growth rate of the reactive layer (diffusion coefficient of atoms, m^2/s), and D_0 is the frequency factor (material constant) (m^2/s). t is the bonding time (time of diffusion of atoms, seconds), k is the reaction constant (m^2/s), Q is the activation energy (Kj/mol), T is the temperature in Kelvin, and R is the universal gas constant (8.314 j/mol-k).

The results of measuring the thickness of areas II and I in the reactive layer of the Zr702/Ti interface at different bonding temperatures based on the results of linear EDS analysis (Figure 2) and using the Digimizer scale measurement software are shown in Table 2. The thickness of the reactive layer (depth of diffusion) was measured in two ways, using linear EDS analysis, which was the result of at least three measurements for each sample, and reporting the average of the results as the final result. Also using the DigiMaizer software. With the increase in the bonding temperature, the thickness of both regions II and I, and as a result the thickness of the reactive layer at the Zr702/Ti interface, has increased. Based on these results, the maximum and minimum thicknesses of the reaction layer, equal to 101 and 38 microns, have been obtained at temperatures of 1050 ℃ and 900 ℃, respectively.

Table 2. The thickness of the reactive layer and the phases formed in the Zr702/Ti interface at different temperatures

Thickness (μ) / Temperature	$(\alpha + \beta)(Zr, Ti)$ (I)	$(\alpha + \beta)(Ti, Zr)$ (II)	Diffusion Zone (DZ)
℃ 1050	45	66	101
℃ 1000	27	47	74
℃ 950	22	39	61
℃ 900	15	24	38

The Ti/Mo interface at different bonding temperatures is shown in Figure 3. The figure clearly shows that at all bonding temperatures, the interdiffusion of the two molybdenum and titanium elements is well done, and the reaction layer (in the form of a dark layer) is formed. The very small difference (less than 7%) of the atomic radii of the two elements, Mo (1.363 angstroms) and Ti (1.462 angstroms), facilitates the formation of a solid solution of molybdenum in titanium and reduces the possibility of the formation of harmful intermetallic compounds. According to the phase diagram of Ti-Mo [24], these two elements form a solid solution at all temperatures and do not form any intermetallic compounds [24]. From SEM images in Figure (3-A) of the Mo/Ti joint interface at 900 °C and 30 minutes duration, the interdiffusion of atoms and two distinct areas can be recognized in the bonding interface. The diffusion behavior of Mo above the β stability line is different from the diffusion of this element below this line [24]. Referring to the equilibrium diagram of Mo-Ti, solid solution phase β_{Ti} is formed at 12 wt% of Mo and $(\alpha + \beta)_{Ti}$ phase is formed at amounts less than 12 wt% of Mo with wavy interface [24-25]. The formation of the solid solution phase β_{Ti} on both sides of the joint interface is attributed to the presence of Mo as a β stabilizing element of the titanium phase, which has been investigated by other researchers [24,26].

The formation of different solid solutions in the reactive layer could be related to the difference in the chemical composition of different points at the reactive layer caused by the difference in the rate of interdiffusion of Ti and Mo atoms. By moving towards the titanium layer and reducing the concentration of molybdenum atoms, the concentration of titanium gradually increases and amounts of β_{Ti} and $(\alpha + \beta)_{Ti}$ begin to nucleate and grow. Therefore, in a range of chemical composition (in the middle of the reactive layer), a two-phase structure is formed and will be stable up to the ambient temperature. The composition of the phases formed in the joint interface is shown in Table (3). The Fig. 3 shows that the wave-shaped interface and numerous holes are formed in the diffusion bonding interface on the side of the molybdenum interlayer, which can be considered as a result of the higher rate of molybdenum diffusion towards the titanium interlayer. More migration of molybdenum elements towards the interlayer of titanium leads to the creation of vacancies on the side of the interlayer of Mo and the formation of C-shaped vacancies at the Mo/Ti interface. These holes are formed at a higher

rate by increasing the diffusion bonding temperature. As a result of voids coalescing, microcracks are formed at the interface of the joint and can reduce the mechanical properties of the joint. At the bonding temperature of 900°C, the measured average thickness of the bonding joints was 1 micron for all phases, which means despite the formation of the reactive layer throughout the interface, the temperature or time of diffusion was not enough to establish the desired bonding.

Comparing the joint interface at temperatures of 950 °C, 1000 °C, and 1050 °C (Figures 3-B, 3-C, and 3-D) revealed that the reactive layer is well formed across the Mo/Ti interface, and at higher temperatures, the average thickness of the diffusion zone has increased as a result of the increase in the diffusion of atoms. The results of the reactive layer thickness in different bonding conditions are presented in Table (4). The results show that by increasing the bonding temperature from 900 °C to 1050 °C, the thickness of the reactive layer has increased from 1 to 1.8 microns. Higher thickness of the reactive layer (diffusion depth) at higher temperature is based on the strong dependence of the diffusion of atoms on temperature, as discussed earlier according to equations 1 and 2 [14, 27]. Increasing the thickness of the reactive layer without forming harmful intermetallic phases leads to a higher level of strength and improves the quality of the bonded joints. Atom migration at higher temperatures, the formation of vacancies in a large volume at the Mo side, and the coalescence of these vacancies lead to Kirkendall hole formation [24]. On the other hand, there is also the possibility of merging vacancies at the interface of solid solution phases $(\alpha + \beta)_{Ti}$ and β_{Ti}. With the increase in the diffusion temperature, the growth of phase $(\alpha + \beta)_{Ti}$ is higher than the growth of phase β_{Ti}, and as a result, the growth of vacancies at the interface of these two phases has increased. At higher temperatures of the diffusion bonding, the diffusion rate of molybdenum atoms towards titanium increases, and a higher number of Kirkendall holes at the diffusion interface will form.
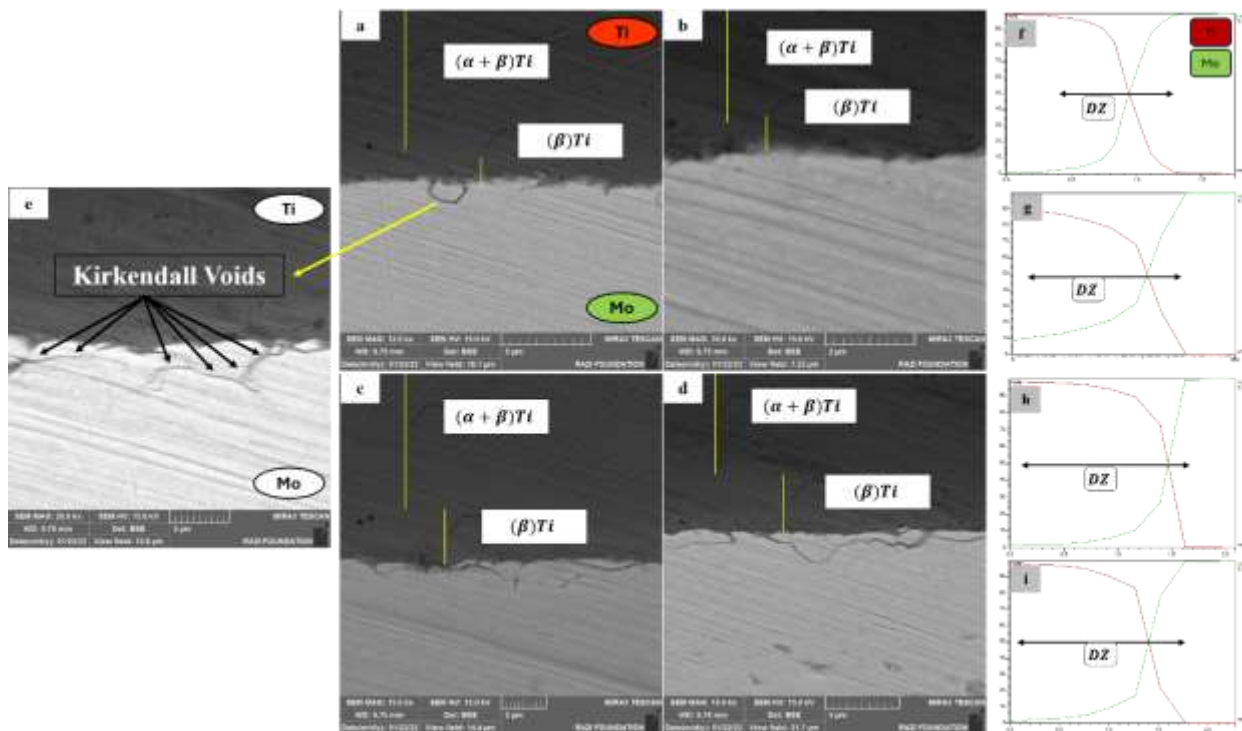

Fig. 3. FESEM images and linear EDS analysis of the joint interface of Mo/Ti at different temperatures –A-E-F - 900 ℃ –B-G - 950 ℃ –C-H - 1000 ℃ –D-I - 1050 ℃

Table 3. EDS analysis of the phases formed in the joint interface of Mo/Ti at temperature 1000 °C and time 30 minutes

Diffusion zone	Mo (%.at)	Ti (%.at)
$(\alpha + \beta)_{Ti}$	10.2	89.8
β_{Ti}	98.9	1.1

Table 4. The thickness of the reactive layer formed in the Mo/Ti at 30 minutes bonding time and different temperatures

Thickness (μ) / Temperature	The total thickness of two areas
℃ 1050	1.8
℃ 1000	1.5
℃ 950	1.2
℃ 900	1

Investigation of the Ni/Mo interface at different bonding temperatures (Figure 4) depicts that at all bonding temperatures, the interdiffusion of Mo and Ni caused the formation of an interlayer without any defects. Due to the small difference between the atomic radii of Mo (1.363 angstroms) and Ni (1.246 angstroms) (less than 9%) [28], the formation of a solid solution of molybdenum in nickel is facilitated, and the formation of harmful intermetallic compounds is possible. Interdiffusion of atoms in the Mo/Ni bonding interface at 900 °C and two distinct regions in light gray and dark gray colors are visible in Fig. 4-A. Based on the information of the equilibrium diagram of Mo-Ni [29] and the results of linear EDS analysis, it be concluded that the solid solution phase of Ni_{Mo} has grown with a completely irregular morphology ($\alpha_{(Ni,Mo)}$) and the intermediate compounds $\delta_{(NiMo)}$, $\gamma_{(Ni_3Mo)}$ and $\beta_{(Ni_4Mo)}$ as well as the solid solution phase of Mo_{Ni} in The joint interface is formed. The diffusion layer formed at the joint interface at all temperatures is composed of $\alpha_{(Ni,Mo)}$ and $\alpha_{(Ni,Mo)} + \beta_{(MoNi_4)}$ and very small areas $\gamma_{(MoNi_3) + \delta_{(MoNi)}}$ was observed [30].

The results of point EDS analysis of the phases formed in the bonding interface in Table (5), showed that the solid solution phase of Mo in Ni ($\alpha_{(Ni,Mo)}$), with amounts greater than 85% by weight of the nickel element with an FCC structure and a completely irregular shape, is formed and the gray light band, in the vicinity of the molybdenum interlayer, is the molybdenum solid solution with a BCC structure. Also, based on the results of linear EDS analysis of the Mo/Ni interface, the phases formed in the vicinity of the interlayer of nickel are considered to be compounds $\beta_{(Ni_4Mo)}$, $\gamma_{(Ni_3Mo)}$ and $\delta_{(NiMo)}$, and the intermediate compound $\delta_{(NiMo)}$ is located in the approximate of Ni-50% Mo zone. The maximum solubility limit of molybdenum in nickel and the formation of a solid solution of nickel is 28.4%, but due to the very low solubility of nickel in molybdenum, the solid solution of nickel in molybdenum in the vicinity of the interlayer of Mo is hardly detectable. This is consistent with the results of other researchers [31-33].
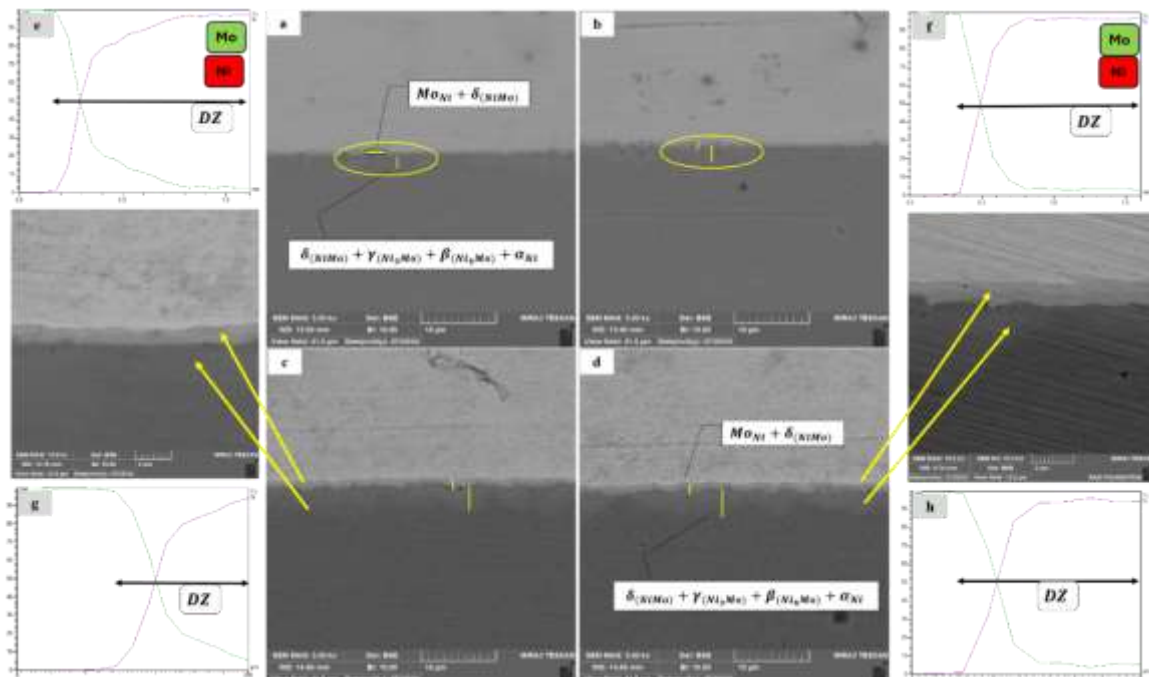

Fig. 4. FESEM images and EDS analysis of the interface of Mo/Ni joint at different temperatures (A-E) - 900 °C, (B-F) - 950 °C, (C-G) - 1000 °C, and (D-H) - 1050 °C

Table 5. EDS analysis of the phases formed in the joint interface of the Mo/Ni at a temperature of 1000 °C and a time of 30 minutes

Diffusion zone	Ni (%.at)
$\alpha_{(Ni,Mo)}$	>85%
$\beta_{(Ni_4Mo)}$ (MoNi$_4$)	80.5~81%
$\gamma_{(Ni_3Mo)}$ (MoNi$_3$)	75.5~76%
$\delta_{(NiMo)}$ (MoNi)	48~52%
Mo_{Ni}	<1%

Comparing the joint interface at different temperatures (950 ℃, 1000 ℃, and 1050 ℃) in Figures 4-B, 4-C, and 4-D shows that with a higher temperature and due to higher diffusion of atoms, the average thickness of the diffusion zone in the Mo/Ni interface increased from 2 microns to a maximum value of 10 microns for different phases (Table 6).

Table 6. The thickness of the Mo/Ni reactive layer in the joint interface at 30 minutes of bonding time and different temperatures

Thickness (μ) / Temperature	Total Thickness	$\delta + \gamma + \beta + \alpha_{Ni}$	$\delta + Mo_{Ni}$
1050 ℃	10	8	2
1000 ℃	8	6.5	1.5
950 ℃	3	2.3	0.7
900 ℃	2	1.5	0.5

In Figure 5, the SEM image of the Ni/SA516 interface at different bonding temperatures shows that proper interdiffusion of atoms in the interface resulted in suitable reactive layer formation. Due to the less than 1% difference between the atomic radius of iron (1.241 angstroms) and nickel (1.246 angstroms), the conditions for the formation of a solid solution of nickel in iron are greatly facilitated, and the possibility of the formation of harmful intermetallic compounds is minimized. Because of the difference in the amount of interdiffusion of Ni and Fe atoms, the joint interface is seen irregularly. The results of EDS analysis of different points of the interface (Figure 5-A) are shown in Table 7. According to the results of EDS analysis and the Fe-Ni equilibrium diagram, it can be stated that the sequence of structures starting from the SA516 side towards Ni is the solid solution of nickel in iron with a BCC structure ($\alpha_{Fe,Ni}$), the solid solution of nickel in iron with the FCC structure (($\gamma_{Fe,Ni}$) and intermetallic compound FeNi$_3$, respectively. The formation of this reactive layer between the nickel and the SA516 base metal creates a suitable bonded joint, which has been confirmed in the results of other researchers [34-35].

From Figure 5-A, it can be seen that the reaction layer has grown in a tooth-shaped (or wave-like) manner, and the thickness of the reaction layer is different in different parts. This phenomenon can be attributed to the strength difference between the base metal and the nickel interlayer. In fact, due to the higher strength and melting point of the SA516 base metal compared to the Ni interlayer and the creation of a heterogamous distribution of thermal stresses, compressive stress and distortion in the interface were caused. This will stretch the interlayer of nickel towards the base metal and increase their contact surface, and therefore the interface becomes wavy [34]. Investigation of EDS results in Figure 5-B of the Ni/A516 interface at 900 ℃ revealed the interdiffusion of atoms and the difference in the diffusion rate of nickel and iron atoms. The results of measuring the thickness of reactive layers at the Ni/A516 interface using the results of linear EDS analysis and Digimizer scale measurement software are presented in Table 7.

By increasing the bonding temperature from 950 ℃ to 1050 ℃, no new intermetallic phases and compounds have been formed, while the interdiffusion of atoms and subsequently the thickness of the reactive layer has increased (Figure 5-C to Figure 5-G). As mentioned earlier, this is according to the equation and the dependence of diffusion on time and temperature. Figure 5-J shows that at the temperature of 1050 C, due to the increase in thermal stresses and, as a result, the residual stress in the connection, physical separation has occurred in this interface.

The results obtained from EDS (Figure 5) and the use of Digimizer scale measurement software presented in Table 7 show that the maximum and minimum

thickness of the SA516/Ni interface reaction layer at temperatures of 900°C and 1050°C are equal to 5 and 15 microns, respectively. A drastic decrease in the thickness of the reactive layer at low temperatures, especially 900°C to about 1 micron, can have a negative effect on the strength of the bonding area. Therefore, it seems that at the bonding temperatures of 900°C and 950°C, despite the formation of a diffusion layer throughout the interface, the bonding temperature is not enough to achieve a proper diffusion depth and establish a joint, especially in the tooth-shaped areas, and a suitable reaction layer with sufficient thickness is not formed. EDS analysis of different phases of the Ni/SA516 interface at the joining temperature (Table 8).
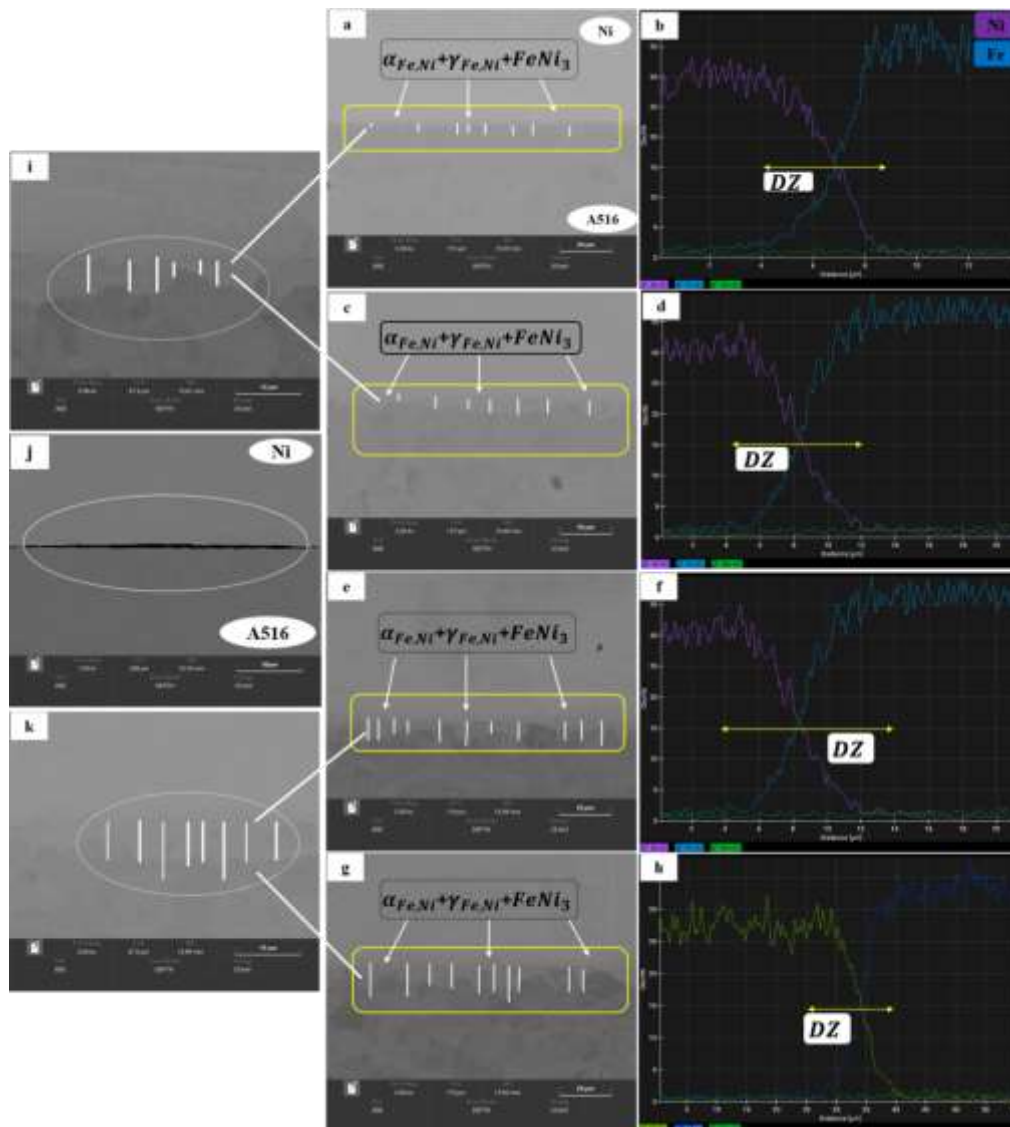

Fig. 5. FESEM images and EDS analysis of the Ni/A516 joint interface at different temperatures (A-B) - 900 °C, (C-D) - 950 °C, (E-F) - 1000 °C, and (G-H-J) - 1050 °C.

Table 7. The thickness of the reactive layer formed at the Ni/A516 joint interface at different bonding temperatures

Thickness (μ) Temperature	Average layer thickness	Maximum layer thickness	Minimum layer thickness
1050 °C	9	15	6.5
1000 °C	7	12	5
950 °C	5.5	8	3.5
900 °C	3.5	5	<3

Table 8. EDS analysis of different phases of the Ni/SA516 interface at the joining temperature

Chemical Compound / Phases	Fe (%.at)	Ni (%.at)
$(\gamma_{Fe,Ni})$	91	8
Ni (SS)	17.5	81.5
$(\alpha_{Fe,Ni} + \gamma_{Fe,Ni} + FeNi_3)$	22.3~99.1	23.3~84.5

4. Conclusion

In this research, the fusion bonding of zirconium alloy 702 to carbon steel G-70 SA516 was performed using a multi-layer interlayer of Ti/Mo/Ni. The results of the studies are briefly as below:

1. The diffusion bonding of Zr702 to A516 steel was successfully done by the SPSDB method and using the Ni/Mo/Ti ternary interlayer at temperatures of 900 ℃ to 1050 ℃. At temperatures lower than 900 ℃ and higher than 1000 ℃, a proper joint was not achieved.

2. The results showed that at 1050 ℃, due to severe thermal stresses and as a result of the residual stress, physical separation occurred at the Ni/A516 interface.

3. The interdiffusion of atoms and the formation of the reactive layer at all of the interfaces of the multilayer joints have occurred. With the increase of the bonding temperature, the interdiffusion of atoms and the thickness of the reactive layer increased in all the joint interfaces, while the formation of a new phase was not observed due to the increase of the bonding temperature. The maximum thickness of the reactive layer of 101 microns was obtained at the Zr702/Ti joint at the bonding temperature of 1050°C and the lowest of 1 micron at the Mo/Ti interface at the bonding temperature of 900°C.

4. It was found that brittle and high-hardness intermetallic phases and compounds are formed at the Ni/Mo interface. While in other interfaces, due to the interdiffusion of atoms, only solid solution was observed in the joint interface.

Reference

[1] B. Zhang, X. Li, T. Wang, and X. Wang, "Microstructure and corrosion behavior of Zr-702 joined by electron beam welding," *Vacuum*, vol. 121, 2015.

[2] S. Yang, J. Cai, P. Lv, C. Zhang, W. Huang, and Q. Guan, "Microstructures and properties of zirconium-702 irradiated by high current pulsed electron beam," *Nucl Instrum Methods Phys Res B*, vol. 358, 2015.

[3] M. M. Atabaki and A. T. Hanzaei, "Partial transient liquid phase diffusion bonding of Zircaloy-4 to stabilized austenitic stainless steel 321," *Mater Charact*, vol. 61, 2010.

[4] A. Lebaili, S. Lebaili, and F. Hodaj, "Interfacial interactions between 304L stainless steel and Zy-4 alloy during isothermal holdings at 1050 °C Interfacial interactions between 304L stainless steel and Zy-4 alloy during isothermal holdings at 1050°C," °C. *Journal of Alloys and Compounds*, vol. 805, 2019.

[5] H. Wang *et al.*, "Diffusion bonding of Zr-2.5Nb zirconium alloy and 304L stainless steel with Nb/Ni hybrid interlayer," *Mater Lett*, vol. 324, 2022.

[6] M. S. Slobodyan, "Methods of Creation of Permanent Zirconium Alloy Joints in Reactor Art: a," 2016.

[7] K. Komuro, "Welding of zirconium alloys," *Welding International*, vol. 8, 1994.

[8] M. Mazar Atabaki, M. E. Bajgholi, and E. H. Dehkordi, "Partial transient liquid phase diffusion bonding of zirconium alloy (Zr-2.5Nb) to stainless steel 321," *Mater Des*, vol. 42, 2012.

[9] X. long Gao, L. kun Li, J. Liu, X. Wang, and H. Yu, "Analysis of Ni interlayer effects on laser beam welding of dissimilar pure Mo alloy to stainless steel," *Int J Refract Metals Hard Mater*, vol. 100, 2021.

[10] K. Bhanumurthy, D. Joyson, S. B. Jawale, A. Laik, and G. K. Dey, "Diffusion Bonding of Nuclear Materials", *BARC Newsl*, 2013.

[11] S. Habisch, M. Böhme, S. Peter, T. Grund, and P. Mayr, "The effect of interlayer materials on the joint properties of diffusion-bonded aluminium and magnesium," *Metals (Basel)*, vol. 8, 2018.

[12] V. Srikanth, A. Laik, and G. K. Dey, "Joining of stainless steel 304L with Zircaloy-4 by diffusion bonding technique using Ni and Ti interlayers," *Mater Des*, vol. 126, 2017.

[13] S. Zeng, G. You, F. Yao, J. Luo, and X. Tong, "Effect of bonding temperature on the microstructure and mechanical properties of the diffusion-bonded joints of Zr705 alloy," *Materials Science and Engineering: A*, vol. 804, 2021.

[14] Z. D. Kadhim, A. I. A.- Azzawi, and S. J. A.-Janabi, "Effect of the Diffusion Bonding Conditions on Joints Strength," vol. 13, 2009.

[15] M. A. Mofid and E. Loryaei, "Effect of bonding temperature on microstructure and intermetallic

compound formation of diffusion bonded magnesium/aluminum joints," *Materwiss Werksttech*, vol. 51, 2020.

[16] B. Zhang, C. Chen, J. He, J. Hou, L. Chai, and Y. Lv, "Spark plasma diffusion bonding of TiAl/Ti2AlNb with Ti as interlayer," *Materials*, vol. 13, 2020.

[17] Q. Li, G. H. Ma, X. Y. Liu, Z. K. Tu, and D. Pan, "Microstructure and mechanical properties of Ti-Nb-Zr alloys prepared by spark plasma sintering," in *Key Engineering Materials*, Trans Tech Publications Ltd, 2017.

[18] W. He, J. Ma, Y. Zhang, H. Wen, and Q. Liu, "Effect of the annealing process on the microstructure and mechanical properties of multilayered Zr/Ti composites," *Materials Science and Engineering: A*, vol. 713, 2018.

[19] J. Lin *et al.*, "Novel Ti-Ta-Hf-Zr alloys with promising mechanical properties for prospective stent applications," *Sci Rep*, vol. 6, 2016.

[20] K. Bhanumurthy, A. Laik, and G. B. Kale, "Novel Method of Evaluation of Diffusion Coefficients in Ti-Zr System," *Defect and Diffusion Forum*, vol. 279, 2008.

[21] A. Cezairliyan and F. Righini, "Thermodynamic studies of the a α -> β phase transformation in zirconium using a sub second pulse heating technique." Institute for materials research, 1975.

[22] Z. Wang, Y. Guo, L. Ren, G. Quan, Y. Liu, and H. Pan, "Effect of Bonding Temperature on Microstructure and Mechanical Properties of 304L/Zircaloy-4 Diffusion-Bonded Joints with Ni/Ta Hybrid Interlayer," *Adv Eng Mater*, vol. 23, 2021.

[23] P. He, J. C. Feng, B. G. Zhang, and Y. Y. Qian, "Microstructure and strength of diffusion-bonded joints of TiAl base alloy to steel." National Key Laboratory of Advanced Welding Production Technology, Harbin Institute of Technology, 2002.

[24] H. Masumoto, K. Nishio, A. Asada, S. Mukae, M. Katoh, and N. Hatanaka, "Diffusion Bonds between Molybdenum and Titanium." Quar. J. JWS 10, 1992.

[25] K. Bhanumurthy, and R. Rainer. "Diffusion bonding of the Mo-base alloy TZM with interlayers." International journal of materials research 99.7, 2008.

[26] P. Duwez, "Effect of Rate of Cooling on the Alpha-Beta Transformation in Titanium and Titanium-Molybdenum Alloys." JOM 3,1951.

[27] B. Chen *et al.*, "Investigation of tungsten/MA956 steel diffusion bonding with an Nb/Ni composite interlayer," *Int J Mod Phys B*, vol. 34, 2020.

[28] S. Guo and C. T. Liu, "Phase stability in high entropy alloys: Formation of solid-solution phase or amorphous phase," *Progress in Natural Science: Materials International*, vol. 21, 2011.

[29] A. Arya, S. Banerjee, G. P. Das, I. Dasgupta, T. Saha-Dasgupta, and A. Mookerjee, "A first-principles thermodynamic approach to ordering in Ni-Mo alloys. *Acta materialia*, *49*, 2001.

[30] C.P. Heijwegen, "Diffusion in the binary systems of molybdenum with nickel, iron and cobalt.", 1973.

[31] J. Zhang, Q. Shen, G. Luo, M. Li, and L. Zhang, "Microstructure and bonding strength of diffusion welding of Mo/Cu joints with Ni interlayer," Mater Des, vol. 39, 2012.

[32] R. E. W. Casselton, W. Hume-Rothery. "The equilibrium diagram of the system molybdenum-nickel." Journal of the Less Common Metals 7.3, 1964.

[33] K. Yaqoob, J. C. Crivello, and J. M. Joubert, "Thermodynamic modeling of the Mo–Ni system," *CALPHAD*, vol. 62, 2018.

[34] H. Sabetghadam, A. Z. Hanzaki, and A. Araee, "Diffusion bonding of 410 stainless steel to copper using a nickel interlayer," Mater Charact, vol. 61, 2010.

[35] L. J. Swartzendruber, V. P. Itkin, and C. B. Alcock, "The Fe-Ni (iron-nickel) system." Journal of phase equilibria 12, 1991.